DESERT

Desert
Online at http://desert.ut.ac.ir

Desert 25-1 (2020) 41-51

Introduction of meta-harzburgites using Contact originated Minerals in the Gishaki ophiolitic area, as a part of Iranian Alpine type ophiolites

B. Bahrambeygi[a], H. Moeinzadeh[a*], S.K. Alavipanah[b]

[a] *Department of Geology, Faculty of Science, Shahid Bahonar University of Kerman, Kerman, Iran*
[b] *Department of Remote Sensing and GIS, Faculty of Geography, University of Tehran, Tehran, Iran*

Received: 12 November 2018; Received in revised form: 12 February 2019; Accepted: 23 February 2019

Abstract

In this paper, we investigated two originated metamorphosed harzburgites of the metaperidotite complex from the northern part of the Gishaki area. Harzburgite rocks, as main ultramafic complexes of the studied area, have outcrops in the scattered locations of the area. Harzburgitic units were discriminated using petrography and Raman spectroscopy. There are two meta-harzburgite types based on the metamorphic history of their protholites with different mineralogy types. Normal metamorphosed harzburgites (N-Hz) are metamorphosed via phases of retrograde processes and contact metamorphosed harzburgites (C-Hz) metamorphosed visa some different phases containing contact metamorphism. One of the best clues that are different in these two rock types is Antigorite mineral characteristics. Antigorite polymorphs have structural and chemical sensitive characteristics that can discriminate using Raman spectroscopy. It had certain specific chemical differentiation compared with other serpentine polymorphs especially in Silica and molecular water contents. Reviewed antigorites illustrated general differentiations in themselves so that polymorphs hosted by C-HZ rocks could be considered as a group with typical Contact antigorite by geochemical criteria such as lower molecular water, higher Octahedral content and, higher Silica content. An increase in Si and Fe^{2+} activities cause incurrences octahedral substitutions as temperature-dependent phenomena in Contact antigorites. Diagrams of Silica versus molecular water contents and octahedral contents clearly distinguished modified antigorites from former antigorite polymorphs. Contact antigorite in the Gishaki serpentinites could be considered as metamorphosed products related to metamorphic aureoles.

Keywords: Gishaki; Ophiolite; Antigorites; Harzburgites; Microprobe

1. Introduction

The retrograde process of serpentinization causes to form serpentine polymorphs, such as antigorite, lizardite, and chrysotile (Dilek *et al*., 2008; Evans, 2004, 2010). Serpentinization is a general retrograde metamorphism characterized by dissolution-precipitation reactions when the ultramafic rocks are fractured and exposed to fluids at crustal levels. Recent studies (Evans *et al*., 2013; Klein *et al*., 2015) have proposed that serpentinization is dominated by incipient hydration involving a volume increase of ~20–40 %, and it consumes water but does not release serpentinization is dominated by incipient serpentinization is dominated by hydration involving a volume increase of ~20–40 %, and it consumes water but does not release any significant dissolved species except for molecular water (Mccollom *et al*., 2009). When primary silicates are changed into serpentines, the density changes from 3.3 to 2.7 g/cm3, and the volume is significantly increased (Bahrambeygi *et al*., 2019). The net result is a fracture system in which newly formed serpentine minerals, particularly the fibrous B polychrome, are formed. Because serpentinite does not expand, it fractures to accommodate the increase in volume (O'hanley, 1992; Surour, 2017; Ulven *et al*., 2014).

* Corresponding author. Tel.: +98 913 1414103
Fax: +98 34 31322035
E-mail address: hmoeinzadeh@uk.ac.ir

The present study aimed to investigate the chemical and mineralogical variations in antigorite types as signs of different phases of contact or normal retrograde metamorphism processes. Petrography, mineral chemistry, and spectral information of serpentinites and metaperidotites were presented along with field and laboratory results. Studies focused on antigorite polymorph characteristics.

1.1. Geological Outline

Ophiolites, belonging to the Late Cretaceous age in, Iran are parts of neotethyan oceanic lithosphere (Robertson, 2002). Some researchers have investigated the mantle sequences of these parts via geochemistry and petrogenetic studies (Alabaster *et al*., 1982; Dilek *et al*., 2007; Floyd *et al*., 1998; Garfunkel, 2006; Godard *et al*., 2006; Godard *et al*., 2003; Robertson, 2002).
The Iranian ophiolite belt, in the parallel zone of the Zagros fold thrust belt, was formed in the southern margin of Eurasia (Shafii Moghadam *et al*., 2010) overextended from northwest to southeast. Tectono-magmatic models presented for Zagros parallel ophiolite belt (including Gishaki area) are different. Some suggest a narrow ocean model (Arvin *et al*., 1994; Arvin *et al*., 1997; Babaie *et al*., 2001; Berberian *et al*., 1982; Davoudzadeh, 1972; Desmons *et al*., 1983; Mccall *et al*., 1982; Şengör, 1990), some are believing to an arc basin model (Delaloye *et al*., 1980; Ghazi *et al*., 2000), and some other presented a back-arc basin model (Agard *et al*., 2006; Shahabpour, 2005). Accordingly, the Gishaki area, located south part of the central Iranian ophiolites on parallel of Zogros zone can considered as south Nain-Baft Ophiolite zone.
Gishaki ophiolite lithologies comprise the components of complete Penrose ophiolites, including tectonized harzburgites, lherzolites, various peridotites, and some pillowed basalts. Figure 1 depicts a local map of the Gishaki area which extends over the southern part of the Nain-Baft ophiolite belt. This map consists of an oceanic mantle and crustal sequences, containing harzburgite, dunite, lherzolite, and some meta-peridotites. According to Watters *et al*. (1970), the ophiolitic zone containing Gishaki ophiolite was covered by Turonian-Maastrichtian (93.5–65.5 Ma) limestone resting conformably on the ophiolite.

The most important ultramafic complexes in the area are tectonized harzburgites as well as minor outcrops of dunite and lherzolite in other geographic parts near the target points. Figure 1 illustrates a local map of the Gishaki area which is irregularly stretched over the southern part of the Nain-Baft ophiolite belt. It is included in the oceanic mantle and crustal sequences which dominantly include meta-harzburgites in the central and northern parts. As shown in Figure 1, the Gishaki area is intensively tectonized with many faults. Different evolutional phenomena can cause geochemical and mineralogical variations in harzburgitic lithologies. The two harzburgites originating from Normally metamorphosed harzburgites (N-HZ) and Contact metamorphosed harzburgites (C-HZ) have the same field characteristics; however, they have different petrographic and geochemistry attributes and different antigorite polymorph types, which is indicative of different Contact and former retrograde metamorphic conditions. Figure 1 shows the metaperidotite and serpentinites that include these two types of harzburgites and the sampled locations.

2. Materials and Methods

To identify the specific antigorites from other serpentine phases, more than 50 samples were examined. Raman spectral patterns that allow for the rapid recognition of mineral polymorphs were used for polymorph classification. In addition to Raman spectroscopy, the petrographic studies and mineral chemistry analysis of samples were executed by the use of scanning electron microscopy (SEM), transmission optical microscopy (TOM), electron microprobe analysis (EMPA), and (in some cases) X-ray powder diffraction (XRD). The microscopic investigation and analytical work were conducted in Iran and Austria at the Geology Department of Bahonar-Kerman University and Department of Lithospheric Sciences at the University of Vienna, respectively.

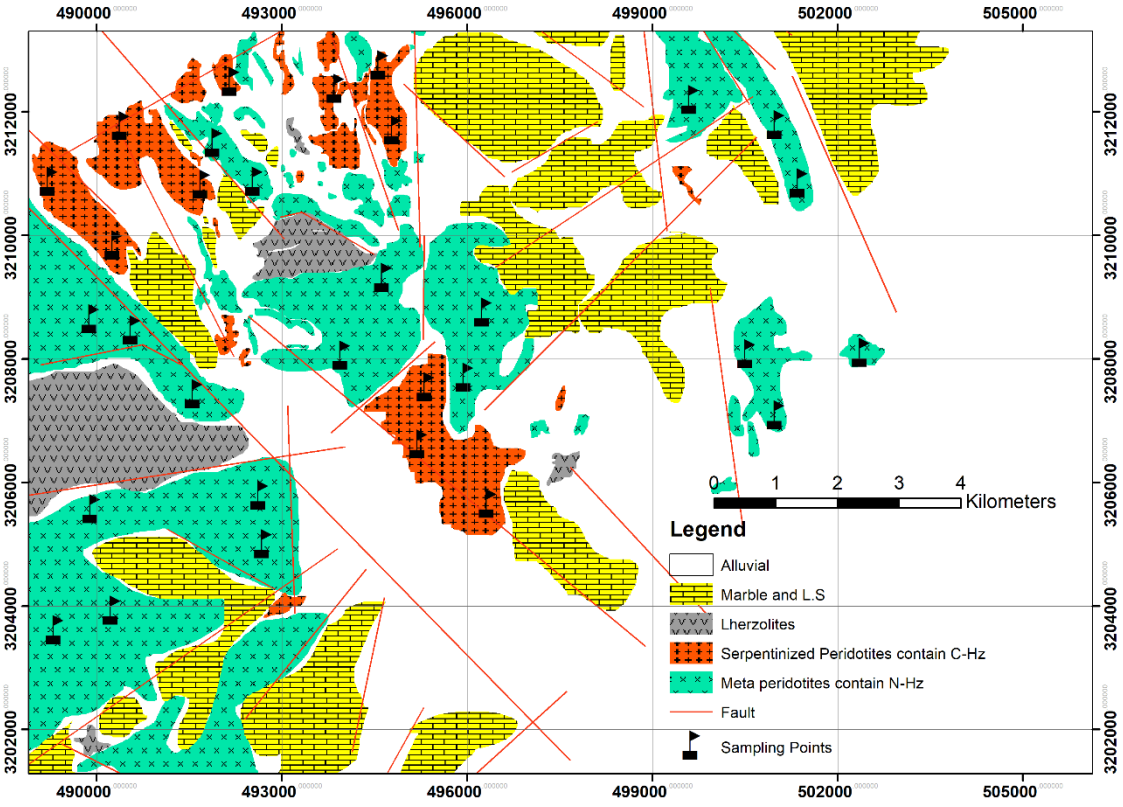

Fig. 1. Local geology map of the Gishaki area, Sampling Points, and location of Contact Harzburgites and Normal Harzburgites

3. Results and Discussion

3.1. Petrographic textural investigation

The background of the studied harzburgitic rocks was represented by serpentine minerals. Antigorites, lizardite, and chrysotile (identified via Raman spectrometry) were the main contextual minerals (Fig. 2). There existed two meta-harzburgites with different pseudomorphism levels: some were non-pseudomorphic with no detectable remnant minerals except for certain spinels. Along with non-pseudomorphic textures (Fig. 2a), there were some pseudomorphic harzburgites with high serpentinization but detectable olivines and pyroxenes occurring with mesh-textured and bastite features (Fig. 2b). Olivines were altered into serpentine minerals with spectral patterns close of lizardite whereas enstatite was altered to serpentine minerals with spectral patterns close to antigorite (Fig. 2b). Other important minerals treated in the present study were pridotitic Cr-spinels whether the rock was normally or Contact metamorphosed (Fig. 2b). Generally, because of their tectonized structures, peridotites in the area were intensively changed. Despite major alteration is serpentinization, but there were some other minor changes such as chloritization and opasitization. Rock types were determined based on the relic pseudomorph minerals and using certain immobile minor elements in the bulk chemistry; therefore, harzburgites were selected. All selected samples had common olivine relics or non-pseudomorphic mesh structures of serpentine minerals. Pseudomorph types were identified in petrography and confirmed with Raman measurements despite major changes (Figs. 3). Two classes of harzburgitic rocks were detected in the studied area. In a class, there was evidence of retrograde metamorphism which led to serpentinization but still remnant mineral surroundings as pseudomorphs even though some Clino-pyroxenes. In some samples associated with the central and western parts of the study area, there were a few clinopyroxene pseudomorphs analyzed with Raman spectroscopy as clinoenstatite. These common meta-harzburgites represented as Normally metamorphosed harzburgites and indexed as N-HZ. Other rock types related to the northern part of the study area had more non-pseudomorphic textures than the first. In this class, there was some evidence related to Contact metamorphisms such as recrystallization structures and low pseudomorph features. In this type, we were unable to find clear surrounding margins as enough reason to call

pseudomorph to altered minerals (Mason *et al*., 1968; Read, 1973; Sinkankas, 1968). These meta-harzburgites represented as Contact metamorphosed harzburgites and were indexed as C-HZ. Regarding antigorite textures, former antigorites were not deformed and were visible as normal fibrous textures (mostly in replaced in OPX pseudomorphs) as could be seen in N-HZ rocks (Fig. 2 and 3). On the contrary, as observed in C-HZ rocks, recrystallized antigorites were deformed as untidy fine-grain textures with no detectable relict minerals (Fig. 3).

Based on Sokkary *et al*. (1985), in comparing the usual type of pseudomorphism through serpentinization, there were other types as Contact metamorphic based pseudomorphism, which could be a reasonable model for C-HZ rocks in the current study. Our suggestion is a metamorphic-based formation model for Contact antigorites. In this type, there are more non-pseudomorphic textures affected by Contact metamorphic processes such as recrystallization.

Table 1. Mineralogy of the studied retrograde metamorphosed harzburgite and Contact metamorphosed harzburgites based on petrography

NO. SAMPLE	GISH-1	GISH-2	GISH-3	GISH-4	GISH-5	GISH-6	GISH-7	GISH-8	GISH-9	GISH-10
ROCK TYPE	N-Harz	C-Harz	C-Harz	N -Harz	C-Harz	C-Harz	C-Harz	N-Harz	N-Harz	N-Harz
ANTIGORITE	High	High	High	Low	High	High	High	High	Moderate	High
LIZARDITE	Moderate	Moderate	Moderate	High	Moderate	Moderate	Moderate	Moderate	Moderate	Moderate
CHRYSOTILE	Low	Moderate	Moderate	Low	Low	Moderate	Low	Moderate	Moderate	Moderate
OPX.	Moderate	Low	Low	Moderate	Low	Low	Low	Moderate	High	Moderate
CPX.	Low	Rare	Rare	Low	Rare	Rare	Rare	Low	Low	Low
OL.	Low	Low	Moderate	Moderate	Low	Low	Low	Moderate	Moderate	Moderate
SPINEL	Moderate	Moderate	Low	Low	Low	Moderate	Low	Low	Moderate	Moderate

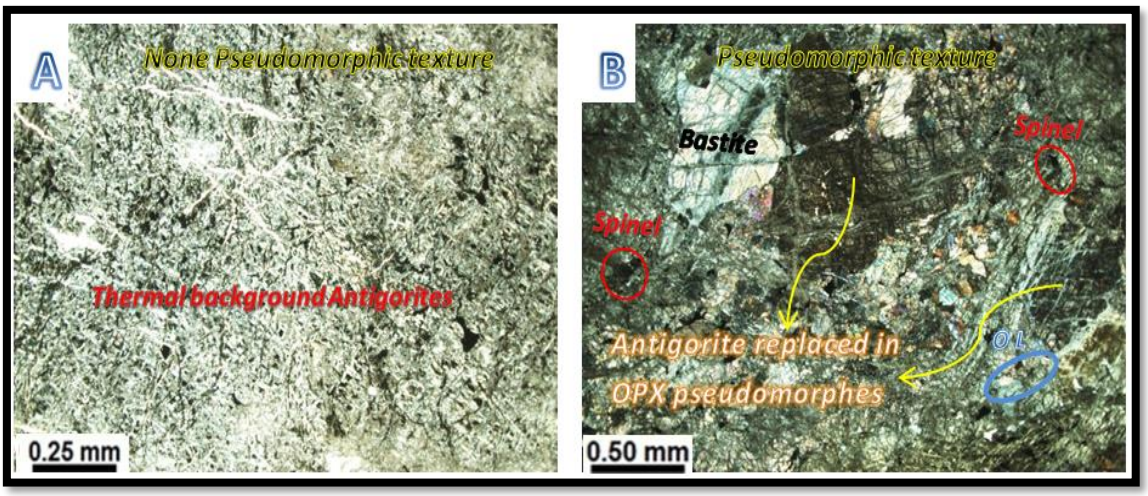

Fig. 2. A) Texture of C-HZ rocks, recrystallized Contact antigorites in background matrix; B) Texture of N-HZ rocks with some pseudomorph minerals such as OL, OPX, and spinels, and fibrous antigorites replaced in OPX pseudomorphs; All microphotographs were taken with Crossed-Nicolls. Abbreviations are based on Whitney *et al*. (2010)

3.2. Raman spectroscopy

The three main minerals of the serpentine group, namely chrysotile, antigorite, and lizardite, have a very similar chemical composition but significantly different structures (Bahrambeygi *et al*., 2019). Spectral patterns provide useful and exact unique chemical and structural characteristics to identify different natural material types (Alavipanah, 2004; Bahrambeygi *et al*., 2017; Bahrambeygi, Moeinzadeh, *et al*., 2012; Bahrambeygi, Ranjbar, *et al*., 2012; Bahrambeygi *et al*., 2013; Bahrambeygi *et al*., 2015; Moeinzadeh, 2015). The naturally-occurring intergrowths of the three types of serpentine minerals are very common. Raman spectroscopy is a precise, simple, and rapid technique that requires no specific sample preparation, which is useful in serpentine polymorph discrimination (Petriglieri *et al*., 2015). Based on Bahrambeygi *et al*. (2019) and Petriglieri *et al*. (2015) there were three main peaks in the Raman spectrum of antigorite minerals. The Peak close to WN of 230 cm-1, and the Peak close to WN of 380 cm-1 and the Peak close to WN of 690 cm-1. The antigorite polymorphs were discriminated based on reference Raman spectra that have been confirmed by several other studies too (Kloprogge *et al*., 2002; Korybska-Sadło *et al*., 2018; Mikouchi *et al*., 2000; Petriglieri *et al*., 2015).

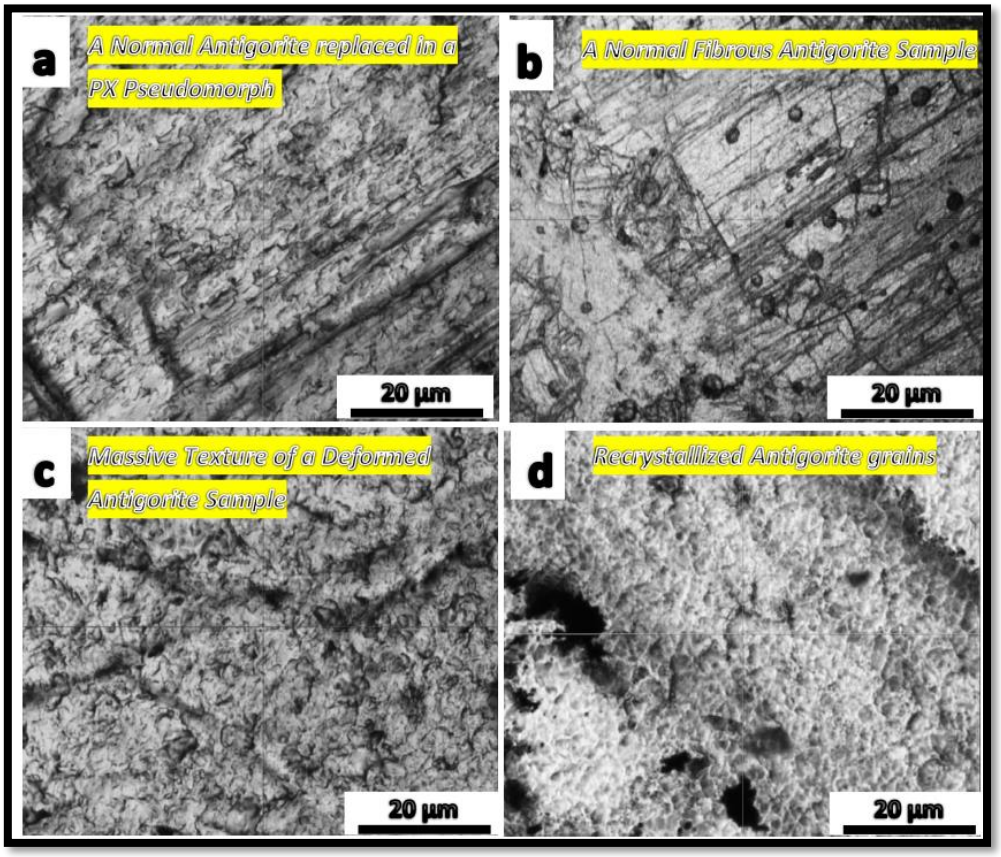

Fig. 3. Some samples of selected point antigorite polymorphs in both N and C harzburgitic rocks under Laser measurement, from the study area.
a) Selected point in a normal antigorite replaced in a PX pseudomorph from an N-HZ sample
b) Selected point in a normal fibrous antigorite sample of Gishaki area from an N-HZ sample
c) Massive texture of a deformed antigorite sample from a C-HZ sample
d) Selected point in recrystallized antigorite grains of a C-HZ sample

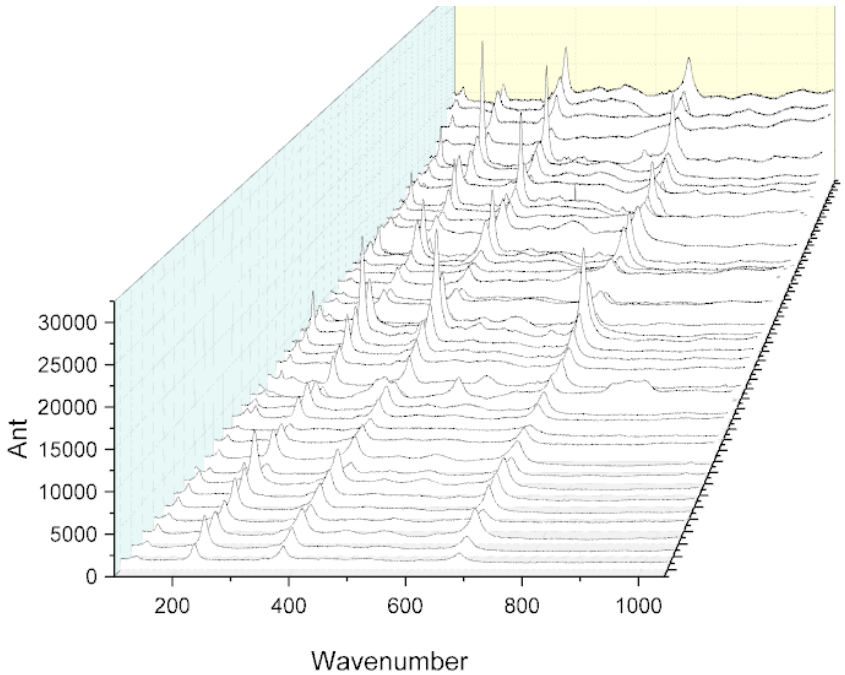

Fig. 4. Range of the main peak on the waterfall diagram of all studied antigorites in the range of antigorite spectral pattern

Table 3. EMPA of antigorite in Harzburgites produced by retrograde and Contact metamorphism (Major oxides in wt. %)

Sample	MgO	SiO2	Al2O3	TiO2	MnO	Cr2O3	FeO	CaO	NiO	Na2O	K2O	Total	H2O
M-Ant-1	40.299	45.087	0.047	0.002	0.026	0.013	3.015	0.07	0.494	0.011	0	88.468	11.136
M-Ant-2	40.131	44.666	0.041	0.01	0.041	0.014	3.086	0.087	0.449	0.013	0.007	88.594	11.455
M-Ant-3	39.835	44.605	0.029	0.007	0.036	0.01	2.901	0.084	0.465	0.001	0.014	88.263	12.013
M-Ant-4	40.18	44.586	0.063	0.008	0.007	0.005	2.958	0.114	0.488	0	0.004	88.843	11.587
M-Ant-5	40.365	44.908	0.034	0	0.028	0.003	2.934	0.093	0.505	0	0.017	88.854	11.113
M-Ant-6	39.832	44.979	0.04	0.007	0.008	0.01	3.071	0.083	0.454	0	0.006	88.726	11.51
M-Ant-7	40.273	44.988	0.041	0	0.026	0	2.867	0.102	0.502	0.002	0.014	88.848	11.185
M-Ant-8	39.896	44.671	0.055	0.008	0.035	0.009	3.098	0.068	0.436	0.006	0.019	88.263	11.699
M-Ant-9	39.876	44.572	0.072	0.002	0.027	0.006	3.102	0.069	0.44	0.009	0	88.699	11.825
M-Ant-10	40.081	44.879	0.001	0.009	0.013	0.004	3.04	0.049	0.435	0.015	0.011	89.129	11.463
M-Ant-11	40.125	44.594	0	0.012	0.041	0	2.828	0.076	0.499	0.015	0.007	88.855	11.803
M-Ant-12	40.184	44.71	0.074	0.009	0.01	0.007	2.877	0.084	0.458	0.005	0.004	87.973	11.578
M-Ant-13	40.179	44.552	0.033	0.009	0.014	0.011	2.968	0.067	0.438	0.007	0.003	88.654	11.719
M-Ant-14	40.017	44.914	0.077	0.007	0.018	0.006	2.928	0.087	0.505	0.005	0.017	87.969	11.419
M-Ant-15	40.112	44.878	0.067	0.009	0.021	0.012	2.87	0.105	0.505	0.004	0.017	89.125	11.411
M-Ant-16	39.873	45.006	0.031	0.006	0.022	0.007	2.927	0.099	0.488	0.001	0.005	88.415	11.535
M-Ant-17	40.399	44.542	0.085	0.008	0.011	0	3.055	0.073	0.501	0.013	0.001	89.175	11.312
M-Ant-18	40.408	45.068	0.053	0.011	0.014	0.013	2.989	0.061	0.492	0.006	0.012	88.726	10.873
M-Ant-19	39.934	44.556	0.08	0.007	0.022	0.002	3.1	0.099	0.483	0.007	0.016	88.089	11.694
M-Ant-20	39.808	45.067	0.045	0.01	0.048	0	2.86	0.051	0.495	0.005	0.006	88.067	11.605
N-Ant-1	40.14	44.057	0.206	0.008	0.019	0	3.679	0.047	0.092	0.006	0.004	87.741	11.742
N-Ant-2	40.478	42.467	0.262	0.011	0.036	0.013	3.515	0.028	0.361	0.006	0.006	86.869	12.817
N-Ant-3	41.137	41.513	0.145	0.006	0.041	0.006	3.394	0.046	0.267	0.004	0.014	87.114	13.427
N-Ant-4	40.276	43.379	0.112	0.002	0.071	0.007	3.322	0.049	0.375	0.008	0.015	87.057	12.384
N-Ant-5	41.008	42.267	0.271	0.012	0.024	0.004	3.375	0.048	0.336	0.009	0.008	87.364	12.638
N-Ant-6	40.275	43.515	0.026	0.012	0.077	0.005	3.733	0.034	0.082	0.008	0.018	88.076	12.215
N-Ant-7	39.997	42.679	0.174	0.009	0.075	0.001	3.226	0.03	0.179	0	0.018	87.111	13.612
N-Ant-8	40.101	43.238	0.193	0.009	0.077	0.011	3.345	0.028	0.124	0.002	0.008	86.861	12.864
N-Ant-9	39.688	42.024	0.213	0.002	0.032	0.012	3.655	0.046	0.153	0.004	0.007	87.452	14.164
N-Ant-10	41.119	42.688	0.103	0.011	0.053	0.003	3.604	0.038	0.267	0.008	0.018	88.186	12.088
N-Ant-11	40.161	41.881	0.318	0.009	0.058	0.013	3.218	0.042	0.193	0.008	0.02	87.361	14.079
N-Ant-12	40.882	41.634	0.323	0.001	0.063	0.003	3.198	0.033	0.193	0.008	0.016	86.933	13.646
N-Ant-13	39.924	43.658	0.025	0.005	0.054	0.011	3.673	0.039	0.16	0.005	0.009	86.288	12.437
N-Ant-14	40.55	43.742	0.024	0.003	0.044	0.011	3.528	0.046	0.284	0.006	0.016	88.205	11.746
N-Ant-15	40.137	43.447	0.264	0.002	0.066	0	3.239	0.058	0.211	0.008	0.002	88.053	12.566
N-Ant-16	39.718	42.564	0.225	0.003	0.063	0.002	3.605	0.053	0.129	0.003	0.004	87.773	13.631
N-Ant-17	40.362	42.084	0.007	0.013	0.032	0.006	3.6	0.046	0.281	0.003	0.005	88.229	13.561
N-Ant-18	40.713	43.739	0.244	0.005	0.016	0.011	3.188	0.029	0.14	0.009	0.018	87.067	11.888
N-Ant-19	40.752	42.445	0.037	0.002	0.016	0.012	3.688	0.045	0.2	0.003	0.01	86.634	12.79
N-Ant-20	40.211	42.966	0.001	0.005	0.071	0.01	3.221	0.056	0.38	0.003	0.013	88.282	13.063
N-Ant-21	41.024	43.972	0.363	0.005	0.026	0.007	3.382	0.043	0.199	0	0.011	87.457	10.968
N-Ant-22	41.139	43.283	0.006	0.012	0.036	0	3.524	0.04	0.138	0	0.002	87.911	11.82
N-Ant-23	40.026	41.49	0.093	0.01	0.029	0.003	3.183	0.051	0.298	0	0	86.411	14.017
N-Ant-24	39.981	43.493	0.277	0.008	0.07	0.009	3.347	0.059	0.218	0.002	0.002	88.032	12.534
N-Ant-25	40.08	43.938	0.057	0.008	0.056	0.012	3.681	0.039	0.096	0.009	0.007	86.85	12.017
N-Ant-26	40.538	41.627	0.002	0.014	0.022	0.007	3.71	0.056	0.351	0	0.009	86.787	13.664

The rest of Table 3. Cations calculated based on the 14 oxygen (anhydrous)

Sample	Mg	Si	Al	Ti	Mn	Cr	Fe	Ca	Ni	Na	K	TOCT	genesis
M-Ant-1	5.481	4.119	0.003	0.000	0.003	0.000	0.230	0.007	0.037	0.002	0.000	5.757	Contact
M-Ant-2	5.495	4.108	0.002	0.000	0.005	0.000	0.237	0.009	0.033	0.002	0.001	5.779	Contact
M-Ant-3	5.481	4.122	0.002	0.000	0.004	0.000	0.224	0.008	0.035	0.000	0.002	5.752	Contact
M-Ant-4	5.508	4.105	0.003	0.000	0.001	0.000	0.227	0.011	0.036	0.000	0.000	5.784	Contact
M-Ant-5	5.501	4.111	0.002	0.000	0.003	0.000	0.224	0.009	0.037	0.000	0.002	5.775	Contact
M-Ant-6	5.450	4.134	0.002	0.000	0.001	0.000	0.236	0.008	0.034	0.000	0.001	5.729	Contact
M-Ant-7	5.489	4.119	0.002	0.000	0.003	0.000	0.219	0.010	0.037	0.000	0.002	5.759	Contact
M-Ant-8	5.475	4.118	0.003	0.000	0.004	0.000	0.238	0.007	0.033	0.001	0.002	5.757	Contact
M-Ant-9	5.481	4.115	0.004	0.000	0.003	0.000	0.239	0.007	0.033	0.002	0.000	5.763	Contact
M-Ant-10	5.481	4.122	0.000	0.000	0.002	0.000	0.233	0.005	0.032	0.003	0.001	5.753	Contact
M-Ant-11	5.508	4.111	0.000	0.000	0.005	0.000	0.218	0.008	0.037	0.003	0.001	5.775	Contact
M-Ant-12	5.503	4.112	0.004	0.000	0.001	0.000	0.221	0.008	0.034	0.001	0.000	5.768	Contact
M-Ant-13	5.513	4.106	0.002	0.000	0.002	0.000	0.228	0.007	0.033	0.001	0.000	5.783	Contact
M-Ant-14	5.471	4.124	0.004	0.000	0.002	0.000	0.225	0.009	0.038	0.001	0.002	5.743	Contact
M-Ant-15	5.482	4.120	0.004	0.000	0.002	0.000	0.220	0.010	0.038	0.001	0.002	5.753	Contact
M-Ant-16	5.454	4.135	0.002	0.000	0.003	0.000	0.225	0.010	0.036	0.000	0.001	5.727	Contact
M-Ant-17	5.526	4.092	0.005	0.000	0.001	0.000	0.234	0.007	0.037	0.002	0.000	5.806	Contact
M-Ant-18	5.492	4.114	0.003	0.000	0.002	0.000	0.228	0.006	0.036	0.001	0.001	5.764	Contact
M-Ant-19	5.484	4.110	0.004	0.000	0.003	0.000	0.239	0.010	0.036	0.001	0.002	5.772	Contact
M-Ant-20	5.446	4.141	0.002	0.000	0.006	0.000	0.219	0.005	0.037	0.001	0.001	5.713	Contact
N-Ant-1	5.530	4.077	0.011	0.000	0.002	0.000	0.284	0.005	0.007	0.001	0.000	5.828	Normal
N-Ant-2	5.672	3.997	0.015	0.000	0.004	0.000	0.276	0.003	0.028	0.001	0.001	5.983	Normal
N-Ant-3	5.810	3.938	0.008	0.000	0.005	0.000	0.269	0.005	0.021	0.001	0.002	6.109	Normal
N-Ant-4	5.594	4.047	0.006	0.000	0.008	0.000	0.259	0.005	0.028	0.001	0.002	5.895	Normal
N-Ant-5	5.736	3.971	0.015	0.000	0.003	0.000	0.265	0.005	0.026	0.002	0.001	6.034	Normal
N-Ant-6	5.583	4.052	0.001	0.000	0.009	0.000	0.290	0.003	0.006	0.001	0.002	5.892	Normal
N-Ant-7	5.631	4.036	0.010	0.000	0.009	0.000	0.255	0.003	0.014	0.000	0.002	5.912	Normal
N-Ant-8	5.595	4.052	0.011	0.000	0.009	0.000	0.262	0.003	0.009	0.000	0.001	5.878	Normal
N-Ant-9	5.643	4.013	0.012	0.000	0.004	0.000	0.291	0.005	0.012	0.001	0.001	5.955	Normal
N-Ant-10	5.712	3.983	0.006	0.000	0.006	0.000	0.281	0.004	0.020	0.001	0.002	6.023	Normal
N-Ant-11	5.701	3.993	0.018	0.000	0.007	0.000	0.256	0.004	0.015	0.001	0.002	5.984	Normal
N-Ant-12	5.782	3.955	0.018	0.000	0.008	0.000	0.254	0.003	0.015	0.001	0.002	6.061	Normal
N-Ant-13	5.544	4.072	0.001	0.000	0.006	0.000	0.286	0.004	0.012	0.001	0.001	5.852	Normal
N-Ant-14	5.591	4.051	0.001	0.000	0.005	0.000	0.273	0.005	0.021	0.001	0.002	5.895	Normal
N-Ant-15	5.580	4.057	0.015	0.000	0.008	0.000	0.253	0.006	0.016	0.001	0.000	5.863	Normal
N-Ant-16	5.604	4.034	0.013	0.000	0.008	0.000	0.285	0.005	0.010	0.001	0.000	5.912	Normal
N-Ant-17	5.699	3.991	0.000	0.000	0.004	0.000	0.285	0.005	0.022	0.001	0.001	6.015	Normal
N-Ant-18	5.614	4.051	0.013	0.000	0.002	0.000	0.247	0.003	0.011	0.002	0.002	5.876	Normal
N-Ant-19	5.704	3.990	0.002	0.000	0.002	0.000	0.290	0.005	0.015	0.001	0.001	6.015	Normal
N-Ant-20	5.626	4.038	0.000	0.000	0.008	0.000	0.253	0.006	0.029	0.001	0.002	5.922	Normal
N-Ant-21	5.610	4.039	0.020	0.000	0.003	0.000	0.259	0.004	0.015	0.000	0.001	5.892	Normal
N-Ant-22	5.680	4.014	0.000	0.000	0.004	0.000	0.273	0.004	0.010	0.000	0.000	5.971	Normal
N-Ant-23	5.728	3.988	0.005	0.000	0.004	0.000	0.255	0.005	0.023	0.000	0.000	6.015	Normal
N-Ant-24	5.560	4.062	0.015	0.000	0.008	0.000	0.261	0.006	0.017	0.000	0.000	5.851	Normal
N-Ant-25	5.537	4.077	0.003	0.000	0.007	0.000	0.285	0.004	0.007	0.002	0.001	5.840	Normal
N-Ant-26	5.744	3.962	0.000	0.001	0.003	0.000	0.295	0.006	0.027	0.000	0.001	6.074	Normal

3.3. Mineral chemistry

Table 1 illustrates the results of electron microprobe analyses of antigorite minerals of Gishaki area. According to Dungan (1979), the structural formula of antigorite calculated on a basis of anhydrous 14(O). The studied antigorite composition listed in Table 1, and by giving an average for total octahedral cations of each type the structural formula for two types is given as follows:

Antigorites in N-Hz: $A_{5.94}\ Si_4O_{10}\ (OH)_8$
Antigorites in C-Hz: $A_{5.74}\ Si_4O_{10}\ (OH)_8$

Where: $A = Mg + Ca + Mn + Fe^{2+} + Ni$

The chemical variations in serpentine polymorphs have been corroborated in many studies Dungan (1979); O'hanley *et al*. (1995); Page (1968). In current study after investigate more than 200 serpentine mineral points via Raman laser analysis we separated about 50 antigorite minerals. The studied antigorites classified based on hosted harzburgitic rocks. They showed different chemical characteristics in Silica, Magnesium, and molecular water contents (Table 1). Generally, as is expected based on previous studies (Dungan (1979); O'hanley *et al*. (1995); Page (1968)) in the current study, antigorites had the highest Silica and Magnesium, the lowest total octahedral

There was some significant dissimilarity between N-HZ and C-Hz antigorite in the structure and composition of the formed antigorite. These special characteristics can be summarized as follows: 1) Silica content of Contact antigorite is relatively high owing to the high silica activity in certain fragments that could belong to the former metamorphic aureoles; 2) the structural formula of antigorites formed in N-HZ is characterized by higher total octahedral cations compared with the antigorite formed in C-HZ; 3) Substitution is recorded in C antigorite is the temperature dependence; 4) the molecular water content in C antigorite is low owing higher rate of dehydration whereas N antigorite generated by retrograde metamorphism contains higher molecular water.

Cations, and low molecular water in comparison with other serpentine polymorphs. Figure 5 shows the places of the studied samples in chemistry discriminant diagrams related to serpentine polymorphs. As illustrated in Figure 5, despite the similar chemical contents of all antigorites, there are some differences between antigorites that are hosted by different harzburgitic rocks too. Antigorites hosted by C-HZ have textural and chemical characteristics close to evidence of a Contact metamorphism phenomenon as shown in some of the previous research (Mellini *et al*., 1987; Surour, 2017; Wunder *et al*., 2001).

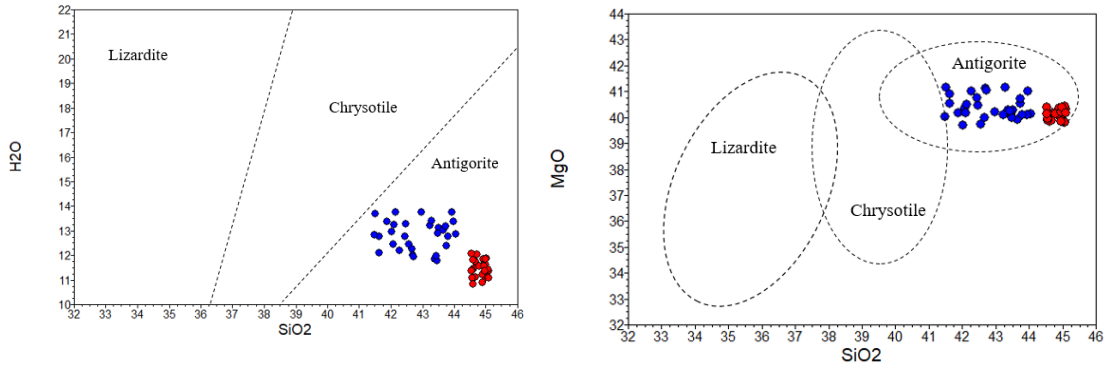

Figure 5: Discriminating diagrams of serpentine polymorphs (by modification from Dungan (1979), O'hanley *et al*. (1995), Page (1968), and Surour (2017) (shape classified) with genetic color classification from normally (Normal) and Contact metamorphosed antigorites (Modified)

The Contact antigorite in the C-HZ rocks of the Gishaki serpentinites is considered as a sign of a Contact metamorphism process in hosted metaperidotite rocks. Contact antigorite could be distinguished by several geochemical factors. High Silica (Table 1) and high formation temperature are ascribed to Silica activity in the granitoid aureole contact. The binary relationship between NiO versus FeO (Fig. 6) was used to distinguish the Contact and normal antigorites. In agreement with Bahrambeygi *et al*. (2019) that studied some other parts in southern of Nain–Baft ophiolites, in current study area also the former antigorites, both Nickel and Iron were high while in normal antigorites, NiO and FeO were low (Fig 6). This could be attributed to the more tendency of Ni to high-temperature phases through the contact metamorphism process.

The obtained results of cation units in the analyzed antigorite samples are listed in Table 2. Silica activity is temperature-dependent because of Contact metamorphism in contact aureole. The presence of tetrahedral substitution in contact antigorite was temperature-dependent. Bahrambeygi *et al.* (2019) Suggest that this is possible despite Al3+ (IV) and Si4+ radius relations because Silica activity in contact aureole is a dominant factor. Based on the collective EMPA data of the studied serpentinites, the antigorite genetic type can be predicted, which has been previously done in other ophiolitic serpentinites in the near of studied area (Bahrambeygi *et al*., 2019) and worldwide Mellini (1986); Mellini *et al*. (2010); Mellini *et al*. (1987). In this scope, factors such as dehydration and Fe, Si, and Ni activities in the same polymorphs can be used as a tracer of the metamorphic type in ophiolitic serpentinites.

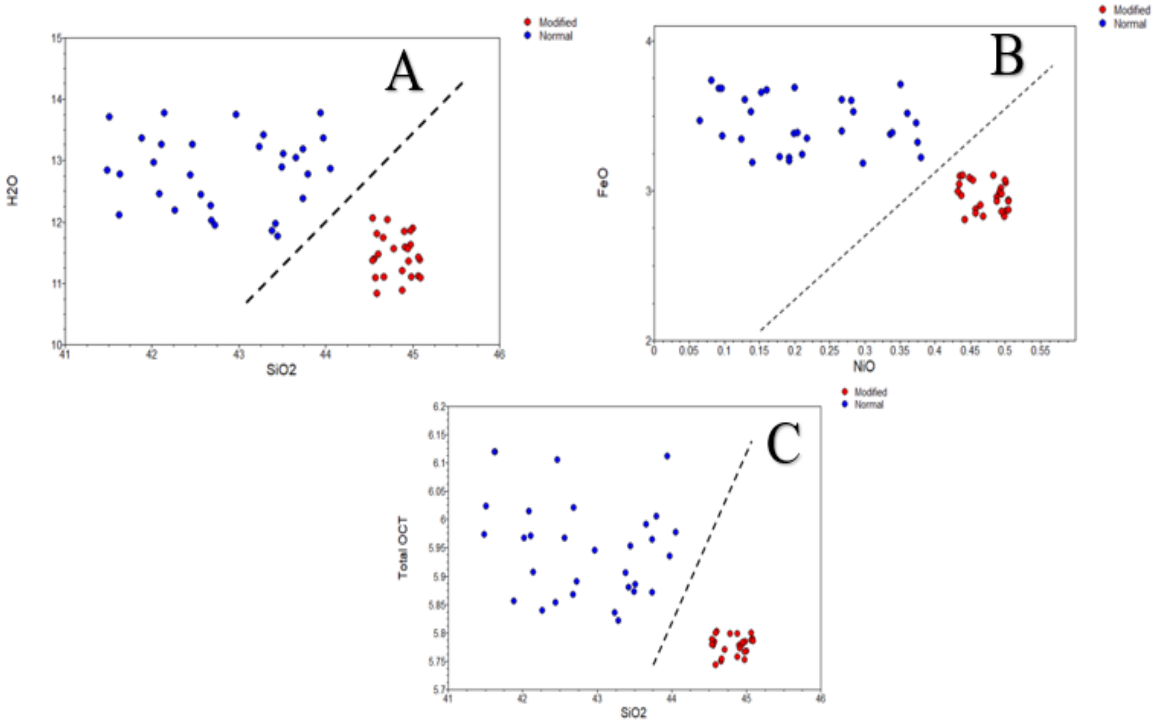

Fig. 6. Contact and normal antigorites in A) Silica versus molecular water diagram; B) NiO versus FeO diagram; C) total octahedral versus Silica diagram (by modification from Surour (2017)

4. Conclusions

Gishaki area located in the Nain-Baft ophiolitic belt contained two types of harzburgitic rocks with different antigorite forms. In some parts of the studied area, there are some meta-harzburgites with Contact evidence and modified antigorite polymorphs. In contrast, there are other normal antigorites formed with the pseudomorphic features of Normally retrograde metamorphosed harzburgites.

Antigorite polymorphs in the Gishaki area recorded normal and Contact metamorphism with different textural and chemical composition features. The results indicated some deformed textures along with relatively higher silica contents, high octahedral cations, and low molecular water contents for certain antigorites occurring in Contact originated harzburgitic rocks.

Tetrahedral substitution occurred in normally formed antigorites but not in Contact types, which is because of the high-temperature condition and silica contents. Therefore, the sum of Si cations was higher around 4 atoms in Contact antigorites owed to silica activity in the contact aureole. In contrast, the substitution in tetrahedral sites happened in normal antigorites with less Si atom activity.

Finally, the present work provided useful discriminating aspects for normal retrograde metamorphosed and Contact metamorphosed antigorite minerals that can be used for metaperidotites and serpentinized complexes in Alpine type ophiolites.

Acknowledgements

The authors are appreciative to Professor R. Abart and the department of Lithospheric

Research in the University of Wien for kind cooperation in running needed analysis.

References

Agard, P., P. Monié, W. Gerber, J. Omrani, M. Molinaro, B. Meyer, P. Yamato, 2006. Transient, synobduction exhumation of Zagros blueschists inferred from P- T, deformation, time, and kinematic constraints: Implications for Neotethyan wedge dynamics. Journal of Geophysical Research: Solid Earth, 111(B11), 152-181.

Alabaster, T., Pearce, J., Malpas, J. 1982. The volcanic stratigraphy and petrogenesis of the Oman ophiolite complex. Contributions to Mineralogy and Petrology, 81(3), 168–183.

Alavipanah, S. 2004. Application of remote sensing and spectroscopy in the earth sciences (soil). University of Tehran press, ISBN, 117.

Arvin, M., P. Robinson, 1994. The petrogenesis and tectonic setting of lavas from the Baft ophiolitic mélange, southwest of Kerman, Iran. Canadian Journal of Earth Sciences, 31(5), 824–834.

Arvin, M., E. Shokri, 1997. Genesis and eruptive environment of basalts from the Gogher ophiolitic mélange, southwest of Kerman, Iran. Ofioliti, 22, 175–182.

Babaie, H., A. Ghazi, A. Babaei, T. La Tour, A. Hassanipak, 2001. Geochemistry of arc volcanic rocks of the Zagros Crush Zone, Neyriz, Iran. Journal of Asian Earth Sciences, 19(1-2), 61-76.

Bahrambeygi, B., H. Moeinzadeh, 2017. Comparison of support vector machine and neutral network classification method in hyperspectral mapping of ophiolite mélanges–A case study of east of Iran. The Egyptian Journal of Remote Sensing and Space Science, 20(1), 1-10.

Bahrambeygi, B., H. Moeinzadeh, S.K. Alavipanah, 2019. Mineralogy, Geochemistry and Raman Spectroscopy of Multi-Genesis Serpentine Polymorphs of Darepahn Ophiolites. Journal of Sciences, Islamic Republic of Iran, 30(3), 251-269.

Bahrambeygi, B., H. Ranjbar, J. Shahabpour, 2012. Comparison of data and spectral driven methods for kaolinite-bearing area mapping in Masahim volcano, using Hyperion images. Journal of Economic Geology, 4(2), 199-215.

Bahrambeygi, B., H. Ranjbar, J. Shahbpour, H. Moeinzadeh, 2015. Study of the scene based atmospheric correction on hyperion images–a case study for recognition of argillic alteration zone in the masahimvolcanic crater. scientific quaternary Journal GeoSciences 24(94), 12-19.

Berberian, F., I. Muir, R. Pankhurst, M. Berberian, 1982. Late Cretaceous and early Miocene Andean-type plutonic activity in northern Makran and Central Iran. Journal of the Geological Society, 139(5), 605–614.

Davoudzadeh, M., 1972. Geology and petrography of the area north of Nain, Central Iran. 162.

Delaloye, M., J. Desmons, 1980. Ophiolites and mélange terranes in Iran: a geochronological study and its paleotectonic implications. Tectonophysics, 68(1-2), 83-111.

Desmons, J., L. Beccaluva, 1983. Mid-ocean ridge and island-arc affinities in ophiolites from Iran: palaeographic implications: complementary reference. Chemical Geology, 39(1-2), 39-63.

Dilek, Y., H. Furnes, M. Shallo, 2007. Suprasubduction zone ophiolite formation along the periphery of Mesozoic Gondwana. Gondwana Research, 11(4), 453-475.

Dilek, Y., H. Furnes, M. Shallo, 2008. Geochemistry of the Jurassic Mirdita Ophiolite (Albania) and the MORB to SSZ evolution of a marginal basin oceanic crust. Lithos, 100(1-4), 174-209.

Dungan, M. A., 1979. A migroprobe study of antigorite and some serpentine pseuipmorphs.

Evans, B. W., 2004. The serpentinite multisystem revisited: chrysotile is metastable. International Geology Review, 46(6), 479-506.

Evans, B. W., 2010. Lizardite versus antigorite serpentinite: Magnetite, hydrogen, and life (?). Geology, 38(10), 879-882.

Evans, B. W., K. Hattori, A. Baronnet, 2013. Serpentinite: what, why, where? Elements, 9(2), 99-106.

Floyd, P., M. Yaliniz, M. Goncuoglu, 1998. Geochemistry and petrogenesis of intrusive and extrusive ophiolitic plagiogranites, Central Anatolian Crystalline Complex, Turkey. Lithos, 42(3-4), 225-241.

Garfunkel, Z., 2006. Neotethyan ophiolites: formation and obduction within the life cycle of the host basins. Geological Society, London, Special Publications, 260(1), 301–326.

Ghazi, M., A. Hassanipak, 2000. Petrology and geochemistry of the Shahr-Babak ophiolite, Central Iran. Geology society of America, 61, 485–498.

Godard, M., D. Bosch, F. Einaudi, 2006. A MORB source for low-Ti magmatism in the Semail ophiolite. Chemical Geology, 234(1-2), 58-78.

Godard, M., J. Dautria, M. Perrin, 2003. Geochemical variability of the Oman ophiolite lavas: Relationship with spatial distribution and paleomagnetic directions. Geochemistry, Geophysics, Geosystems, 4(6), 281–298.

Klein, F., N.G. Grozeva, J.S. Seewald, T.M. McCollom, S.E. Humphris, B. Moskowitz, W.A. Kahl, 2015. Experimental constraints on fluid-rock reactions during incipient serpentinization of harzburgite. American Mineralogist, 100(4), 991-1002.

Kloprogge, J. T., D. Wharton, L. Hickey, R.L. Frost, 2002. Infrared and Raman study of interlayer anions CO32−, NO3−, SO42− and ClO4− in Mg/Al-hydrotalcite. American Mineralogist, 87(5-6), 623-629.

Korybska-Sadło, I.,G. Gil, P. Gunia, M. Horszowski, M. Sitarz, 2018. Raman and FTIR spectra of nephrites from the Złoty Stok and Jordanów Śląski (the Sudetes and Fore-Sudetic Block, SW Poland). Journal of Molecular Structure, 1166, 40-47.

Mason, B., L.G. Berry, 1968. Elements of mineralogy. Retrieved from

McCall, G., R. Kidd, 1982. The Makran, Southeastern Iran: the anatomy of a convergent plate margin active from Cretaceous to Present. Geological Society, London, Special Publications, 10(1), 387–397.

Mccollom, T. M., W. Bach, 2009. Thermodynamic constraints on hydrogen generation during serpentinization of ultramafic rocks. Geochimica et Cosmochimica Acta, 73(3), 856-875.

Mellini, M., 1986. Chrysotile and polygonal serpentine from the Balangero serpentinite. Mineral Mag, 50, 301-306.

Mellini, M., G. Cressey, F. Wicks, B. Cressey, 2010. The crystal structure of Mg end-member lizardite-1 T

forming polyhedral spheres from the lizard, Cornwall. Mineralogical Magazine, 74(2), 277–284.

Mellini, M., V. Trommsdorff, R. Compagnoni, 1987. Antigorite polysomatism: behaviour during progressive metamorphism. Contributions to Mineralogy and Petrology, 97(2), 147-155.

Mikouchi, T., M. Miyamoto, 2000. Micro Raman spectroscopy of amphiboles and pyroxenes in the martian meteorites Zagami and Lewis Cliff 88516. Meteoritics & Planetary Science, 35(1), 155-159.

Moeinzadeh, H., 2015. Hyperspectral mapping of Iranian east ophiolite mélanges using neutral network classification method. Arabian Journal of Geosciences, 8(4), 2169-2178.

O'Hanley, D. S., 1992. Solution to the volume problem in serpentinization. Geology, 20(8), 705-708.

O'Hanley, D. S., F.J. Wicks, 1995. Conditions of formation of lizardite, chrysotile and antigorite, Cassiar, British Columbia. Canadian Mineralogist, 33(4), 753-773.

Page, N. J., 1968. Serpentinization in a sheared serpentinite lens, Tiburon Peninsula, California. US Geological Survey Professional Paper, 600, 21-28.

Petriglieri, J., E. Salvioli- Mariani, L. Mantovani, M. Tribaudino, P. Lottici, C. Laporte- Magoni, D. Bersani, 2015. Micro Raman mapping of the polymorphs of serpentine. Journal of Raman Spectroscopy, 46(10), 953-958.

Read, H. H., 1973. Rutley's Elements of Mineralogy: Springer.

Robertson, A., 2002. Overview of the genesis and emplacement of Mesozoic ophiolites in the Eastern Mediterranean Tethyan region. Lithos, 65(1-2), 1–67.

Şengör, A., 1990. A new model for the late Palaeozoic—Mesozoic tectonic evolution of Iran and implications for Oman. Geological Society, London, Special Publications, 49(1), 797–831.

Shafii Moghadam, H., R.J. Stern, M. Rahgoshay, 2010. The Dehshir ophiolite (central Iran): Geochemical constraints on the origin and evolution of the Inner Zagros ophiolite belt. Bulletin, 122(9-10), 1516-1547.

Shahabpour, J., 2005. Tectonic evolution of the orogenic belt in the region located between Kerman and Neyriz. Journal of Asian Earth Sciences, 24(4), 405-417.

Surour, A. A., 2017. Chemistry of serpentine "polymorphs" in the Pan-African serpentinites from the Eastern Desert of Egypt, with an emphasis on the effect of superimposed thermal metamorphism. Mineralogy and Petrology, 111(1), 99-119.

Ulven, O., H. Storheim, H. Austrheim, A. Malthe-Sørenssen, 2014. Fracture initiation during volume increasing reactions in rocks and applications for CO2 sequestration. Earth and Planetary Science Letters, 389, 132-142.

Watters, W., M. Sabzehei, 1970. Preliminary report, geology and topography of the metamorphic and igneous complex of the central part of the Neyriz Quadrangle. Geol. Surv. Iran, Int. Rep, 253–269.